

**Structures and magnetic properties of two heterometallic Cu(II)-Cd(II) polymers
exhibiting antiferromagnetic ordering**

Zhong-Yi Li,* Ran Zhang, Peng-Yu Zhu, Chi Zhang, Dong-Qing Wu and Bin Zhai*

Materials and physical measurements

All chemicals were purchased from commercial sources and used without further purification. FT-IR spectrums were recorded in the range of 4000-400 cm⁻¹ on a JASCO FT/IR-430 spectrometer with KBr pellet. Elemental analyses were determined by a Vario EL III elemental analyzer. Thermogravimetric analyses were performed under a flow of nitrogen (20 mL/min) at a ramp rate of 10 °C/min, using a NETZSCH STA 449F3 instrument. Powder X-ray diffraction (PXPD) measurements were carried out on a Bruker D8 ADVANCE X-ray Diffractometer using Cu K α ($\lambda = 1.5418 \text{ \AA}$) at room temperature. Magnetic measurements were carried out on a Quantum Design SQUID magnetometer MPMS XL-7. The data were corrected for the sample holder and the diamagnetic contributions.

Table S1. Selected bond lengths (\AA) and angles ($^\circ$) for **1**.

Cd(1)-O(1)	2.324(2)	Cu(1)-O(4)	1.987(2)
Cd(1)-O(3) ^{#2}	2.389(2)	Cu(1)-N(1) ^{#4}	1.995(2)
Cd(1)-O(4) ^{#2}	2.466(2)	Cu(1)-O(2)	2.008(2)
Cd(1)-O(2)	2.563(2)	Cu(1)-O(7)	2.279(2)
Cu(1)-O(5)	1.941(2)		
O(1)-Cd(1)-O(3) ^{#3}	117.49(7)	O(4)-Cu(1)-O(2)	86.92(8)
O(1)-Cd(1)-O(1) ^{#1}	119.77(11)	O(4) ^{#3} -Cd(1)-O(2)	87.91(7)
O(3) ^{#2} -Cd(1)-O(3) ^{#3}	127.86(11)	O(1)-Cd(1)-O(3) ^{#2}	88.82(7)
O(3) ^{#2} -Cd(1)-O(2)	141.82(7)	O(5)-Cu(1)-O(7)	89.58(9)
O(1)-Cd(1)-O(4) ^{#2}	142.51(7)	O(3) ^{#2} -Cd(1)-O(4) ^{#3}	90.05(7)
Cu(1)-O(2)-Cd(1)	151.44(10)	O(4)-Cu(1)-N(1) ^{#4}	90.08(9)
O(4) ^{#2} -Cd(1)-O(2)	164.30(7)	O(2)-Cu(1)-O(7)	90.17(9)
O(5)-Cu(1)-O(4)	174.25(9)	O(5)-Cu(1)-O(2)	91.28(9)
N(1) ^{#4} -Cu(1)-O(2)	176.15(9)	O(5)-Cu(1)-N(1) ^{#4}	91.48(10)
O(1)-Cd(1)-O(2)	53.08(7)	N(1) ^{#4} -Cu(1)-O(7)	92.53(9)
O(3) ^{#2} -Cd(1)-O(4) ^{#2}	53.69(7)	O(2) ^{#1} -Cd(1)-O(2)	92.98(10)
O(3) ^{#3} -Cd(1)-O(2)	79.58(7)	O(4) ^{#3} -Cd(1)-O(4) ^{#2}	95.45(10)
O(1)-Cd(1)-O(4) ^{#3}	83.20(7)	O(4)-Cu(1)-O(7)	95.88(9)
O(1) ^{#1} -Cd(1)-O(2)	84.82(7)	□	□

Symmetry codes: #1 -x+1, y, -z+1/2; #2 x, -y+2, z-1/2; #3 -x+1, -y+2, -z+1; #4 x, -y+1, z+1/2.

Table S2. Selected bond lengths (\AA) and angles ($^\circ$) for **2**.

Cd(1)-O(1)	2.262(3)	Cu(1)-O(2)	1.935(3)
Cd(1)-O(5)	2.313(3)	Cu(1)-O(4)	1.952(3)
Cd(1)-O(6)	2.317(3)	Cu(1)-O(7)	2.503(1)
O(1) ^{#1} -Cd(1)-O(1)	180	O(6)-Cd(1)-O(6) ^{#1}	180.00(15)
O(5)-Cd(1)-O(5) ^{#1}	180	O(2)-Cu(1)-O(2) ^{#2}	180.00(6)
O(1)-Cd(1)-O(6) ^{#1}	103.28(12)	O(4) ^{#2} -Cu(1)-O(4)	180.00(11)
O(5)-Cd(1)-O(6) ^{#1}	91.31(13)	O(1)-Cd(1)-O(6)	76.72(12)
O(2)-Cu(1)-O(4)	92.80(13)	O(2)-Cu(1)-O(4) ^{#2}	87.20(13)
O(1)-Cd(1)-O(5) ^{#1}	89.25(13)	O(5)-Cd(1)-O(6)	88.69(13)
O(1)-Cd(1)-O(5)	90.75(13)		

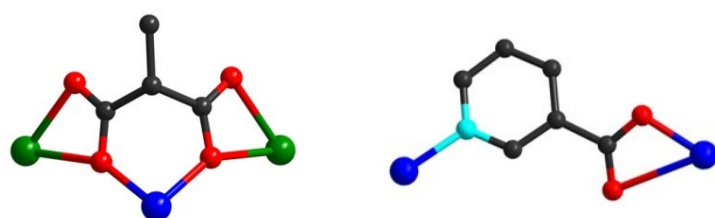
Symmetry codes: #1 -x+1, -y, -z+1 #2 -x+1, -y, -z+2.

Table S3. Selected hydrogen bond lengths (\AA) and bond angles ($^\circ$) in **1**.

D-H	d(D-H)	d(H..A)	\angle DHA	d(D \cdots A)	A	Symmetry Code
O7-H7A	0.857	2.012	167.6	2.855	O1	[-x+1, -y+2, -z+1]
O7-H7B	0.869	2.179	155.73	2.993	O3	[-x+1, -y+2, -z+1]

Table S4. Selected hydrogen bond lengths (\AA) and bond angles ($^\circ$) in **2**.

D-H	d(D-H)	d(H..A)	\angle DHA	d(D \cdots A)	A	Symmetry Code
O5-H5B	0.842	1.923	159.61	2.728	O9	
O5-H5A	0.842	1.889	165	2.711	O3	[x+1, y, z-1]
O6-H6B	0.844	1.987	162.9	2.804	O8	
O6-H6A	0.84	2.325	124.33	2.884	O2	[-x+1, -y, -z+1]
O6-H6A	0.84	2.595	143.58	3.309	O4	[x, y, z-1]
O6-H6A	0.84	2.429	136.97	3.097	O7	[x, y, z-1]
O7-H7B	0.848	2.061	165.31	2.889	O8	[-x+1, -y+1, -z+1]
O7-H7A	0.842	2.045	167.57	2.872	O3	[x+1, y, z]
O9-H9B	0.849	2.047	166.22	2.879	O4	[-x+1, -y, -z+2]
O9-H9A	0.839	2.246	144.18	2.967	O1	[x+1, y, z]
O9-H9A	0.839	2.517	142.78	3.225	O6	[x+1, y, z]
O8-H8B	0.848	2.141	145.22	2.878	O5	
O8-H8A	0.848	2.069	150.86	2.84	O9	[-x+1, -y+1, -z+1]

**Fig. S1** Coordinate modes of MMA^{2-} and NTA^- ligands in **1**.

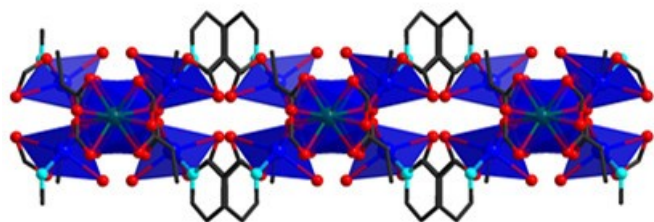


Fig. S2 The 2D structure of **1** viewed along *c* axis.

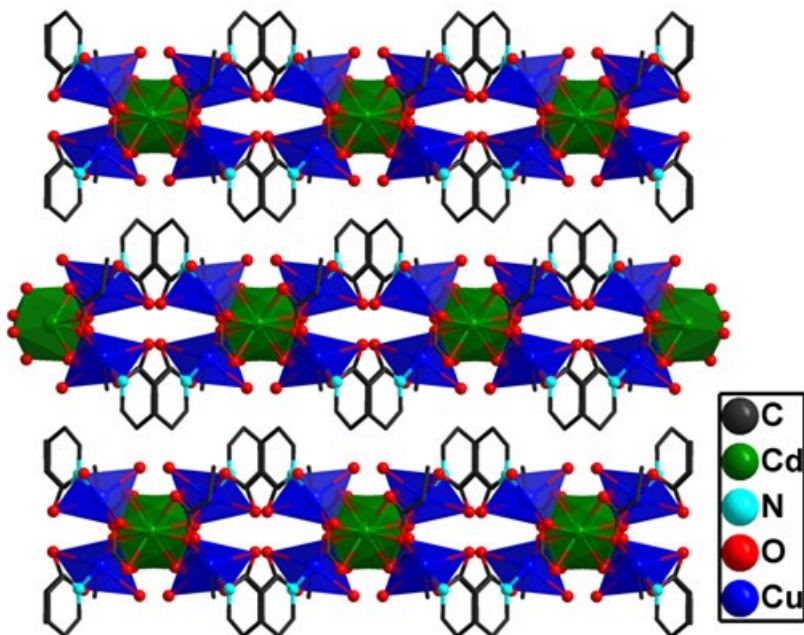


Fig. S3 The packing diagram of the 2D structure of **1** viewed along *c* axis.

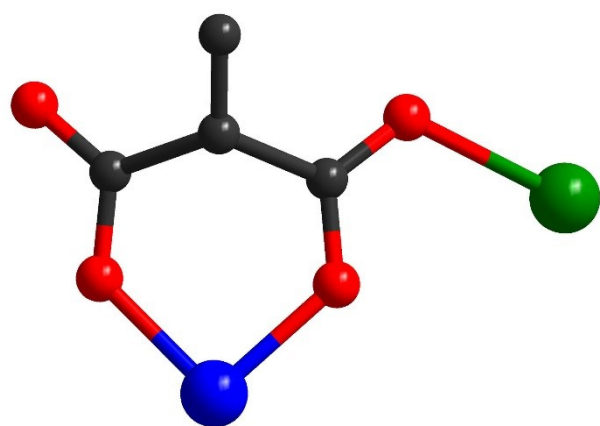


Fig. S4 Coordinate mode of MMA²⁻ ligand in **2**.

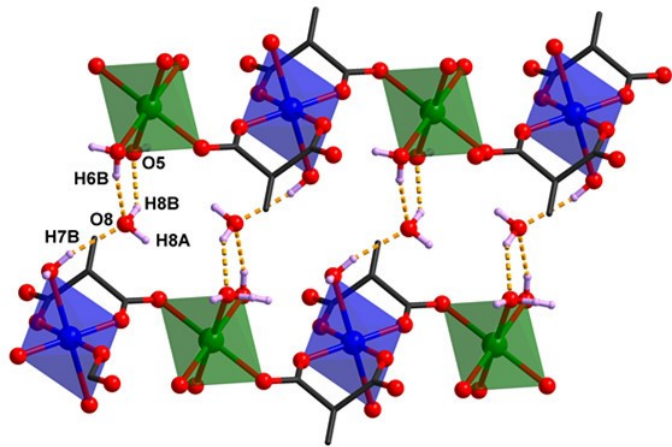


Fig. S5 The 2D hydrogen-bond network of **2** between the adjacent 1D chains in the *bc* plane.

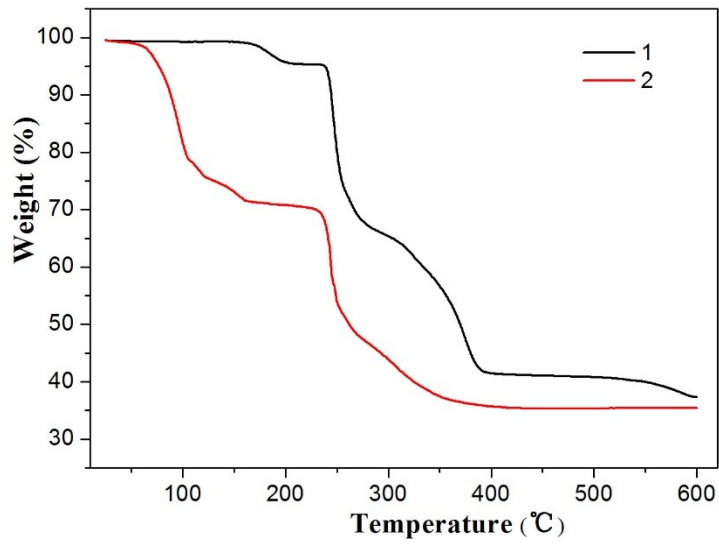
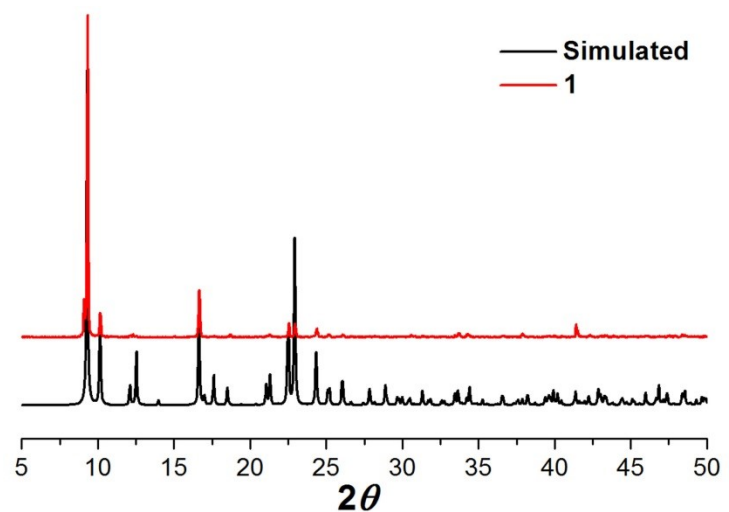
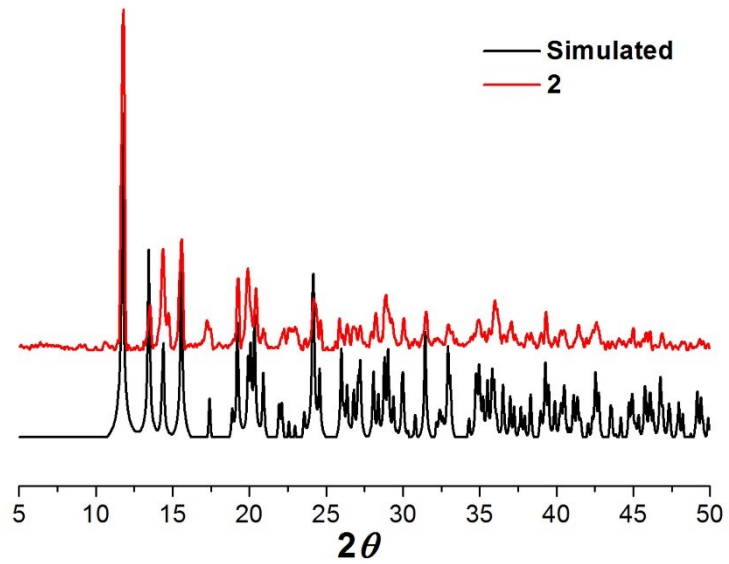


Fig. S6 TGA curves for **1** and **2** in a nitrogen atmosphere (10 °C/min).



Fig, S7 Powder X-ray diffraction pattern of **1**.



Fig, S8 Powder X-ray diffraction pattern of **2**.

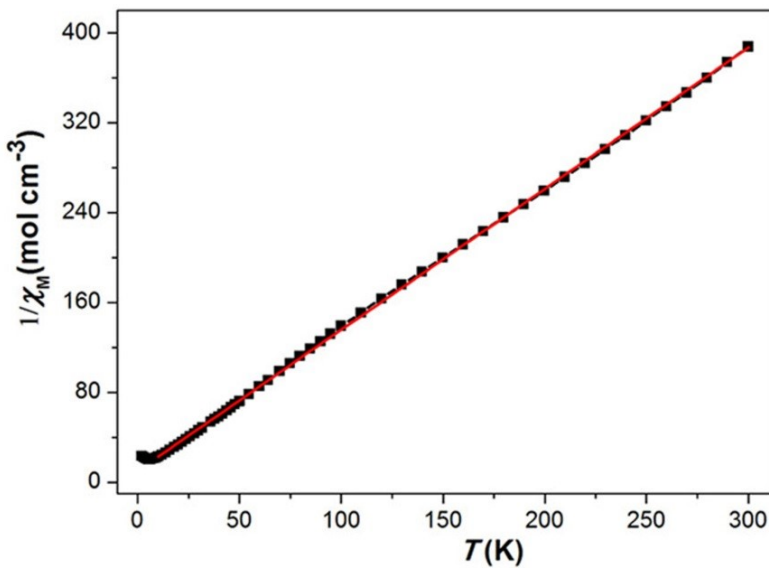


Fig. S9 Temperature dependence of the $1/\chi_M$ values for **1** at 1000 Oe dc magnetic field. The red solid line represents the best fit to the data between 10 and 300 K.

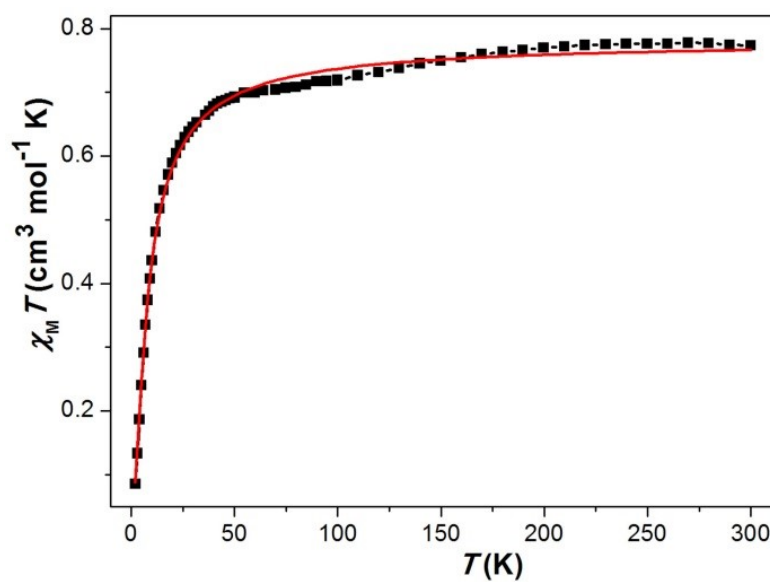


Fig. S10 The best fit to the data of the temperature dependence of the $\chi_M T$ values for **1** based on the dinuclear $[\text{Cu}_2]$ -based 1D model with the inter-chain interactions.

The fitting equations based on the mononuclear Cu²⁺ model:

$$\chi = \frac{Ng^2\beta^2}{3kT} \quad (1)$$

$$\chi_M = \frac{\chi}{1 - (2zJ' / Ng^2\beta^2)\chi} \quad (2)$$

The fitting equations based on the discrete dinuclear [Cu₂] cluster model with the Hamiltonian H= -2JΣS₁S₂:

$$\chi_d = \frac{2Ng^2\beta^2}{kT} \times \frac{1}{3 + e^{-2J/kT}} \quad (3)$$

$$\chi_M = \frac{\chi_d}{1 - (2zJ' / Ng^2\beta^2)\chi_d} \quad (4)$$

Table S5. The parameters of the best fitting based on different models.

Parameters	Mononuclear model	Dinuclear [Cu ₂] cluster model	[Cu ₂]-based 1D model		
<i>g</i>	2.93(1)	2.00(1)	2.05(1)	2.04(1)	2.04(1)
<i>zJ'</i> / cm ⁻¹	-12.03(1)	-	-3.21(1)	-	0.12(1)
<i>J</i> (<i>J</i> _d) / cm ⁻¹	-	-4.42(1)	-2.91(1)	-1.36(1)	-1.39(1)
<i>J</i> _c / cm ⁻¹	-	-	-	-1.75(1)	-1.77(1)
<i>R</i>	1.15×10 ⁻³	1.74×10 ⁻³	3.20×10 ⁻⁴	1.95×10 ⁻⁴	1.95×10 ⁻⁴

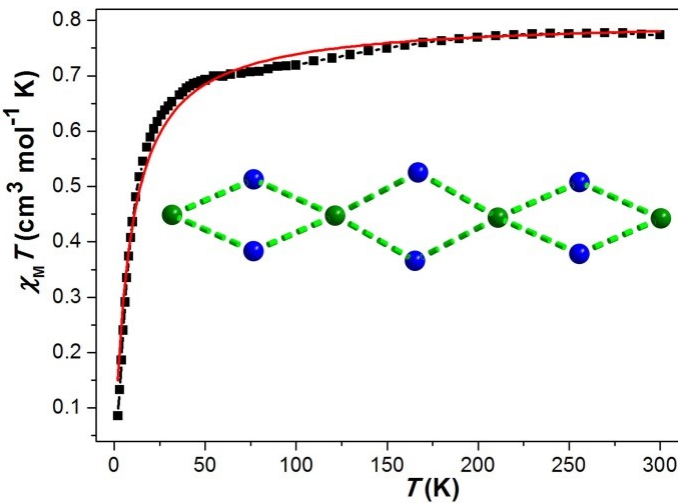


Fig. S11 The best fit to the data of the temperature dependence of the $\chi_M T$ values for **1** based on the discrete mononuclear Cu^{2+} model (inset) with the interactions between the neighboring Cu^{2+} ions.

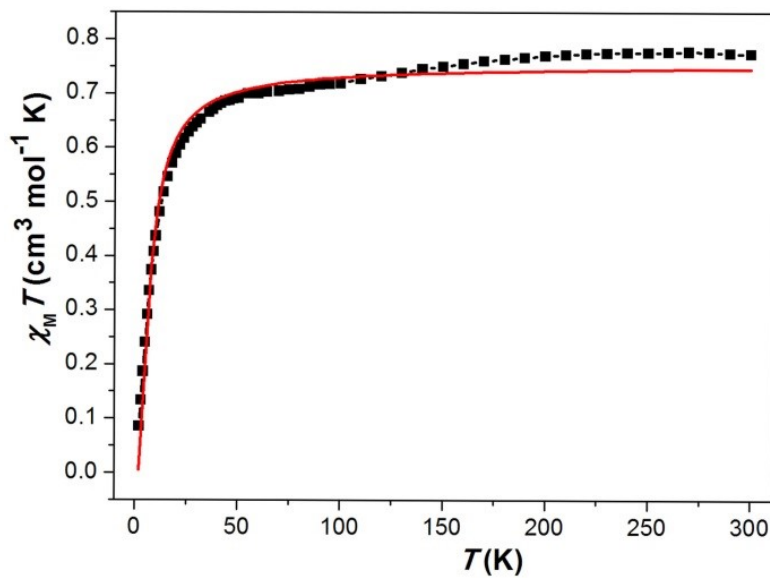


Fig. S12 The best fit to the data of the temperature dependence of the $\chi_M T$ values for **1** based on the discrete dinuclear $[\text{Cu}_2]$ cluster model without the inter-cluster interactions.

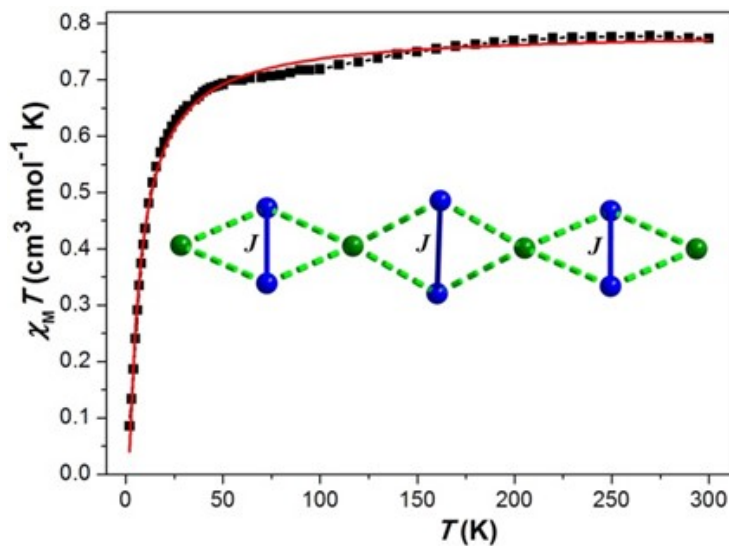


Fig. S13 The best fit to the data of the temperature dependence of the $\chi_M T$ values for **1** based on the discrete dinuclear $[\text{Cu}_2]$ cluster model with the inter-cluster interactions.

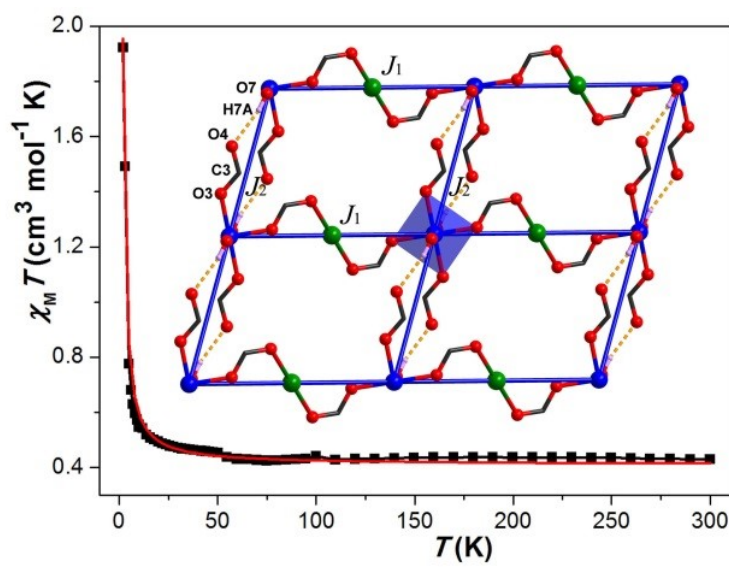


Fig. S14 Temperature dependence of the $\chi_M T$ data for **2** at 1000 Oe dc magnetic field. The red solid line represents the best fit to the data based on the 2D grid model with different coupling parameters. Inset: Schematic diagram of the magnetic exchange pathways of the 2D grid model.

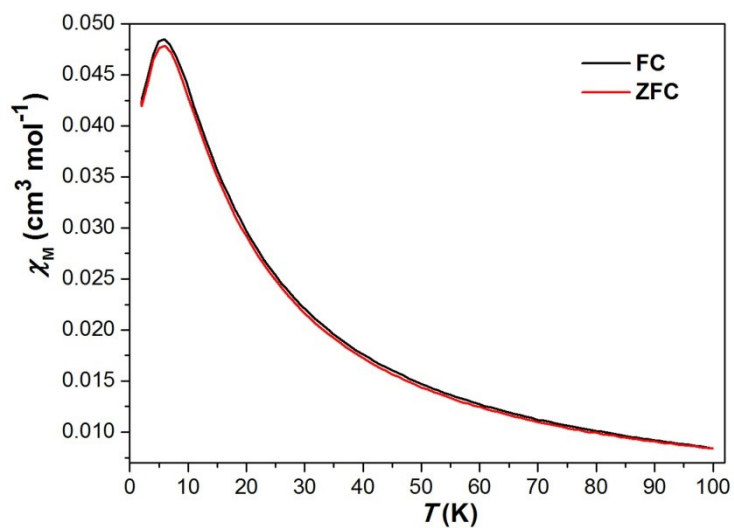


Fig. S15 FC and ZFC magnetization curves of **1** at 100 Oe.

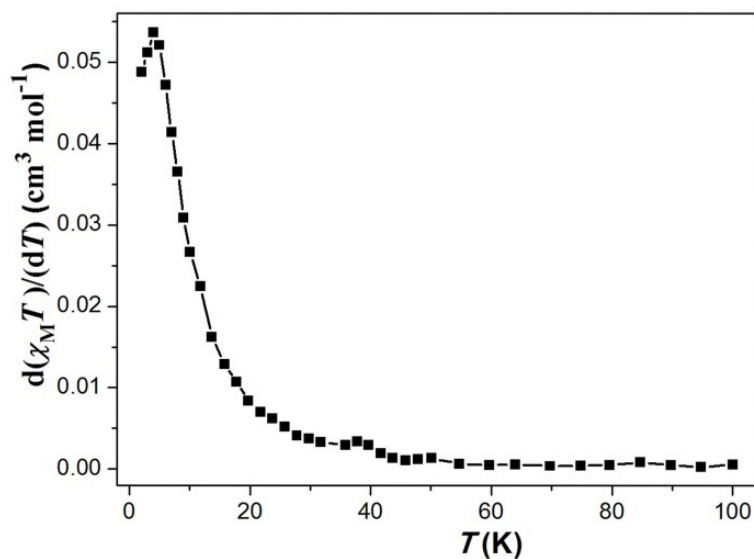


Fig. S16 Plot of the temperature dependence of $d(\chi_m T)/dT$ of **1** measured at a 1000 Oe field.

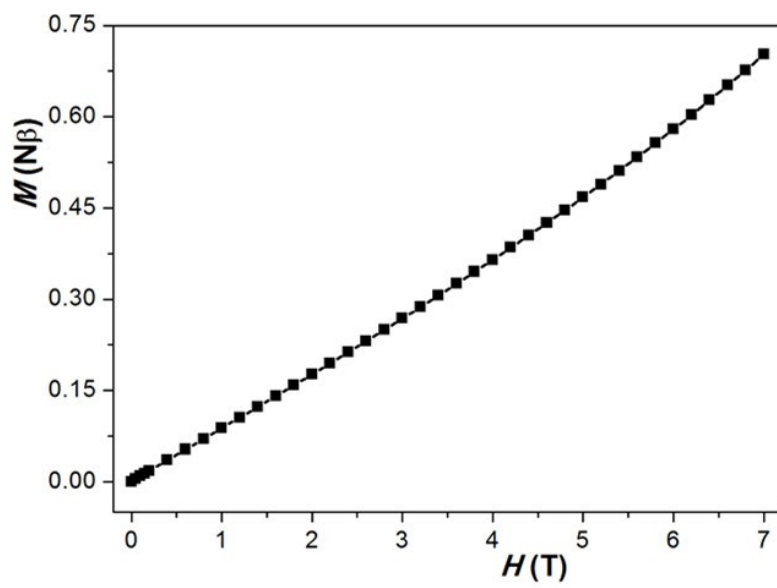


Fig. S17 Magnetization *versus* applied magnetic field at 2.0 K for **1**.

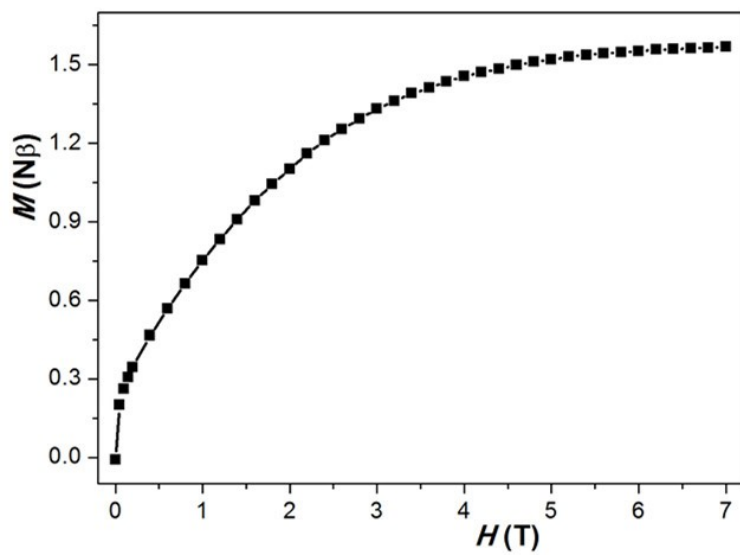


Fig. S18 Magnetization *versus* applied magnetic field at 2.0 K for **2**.

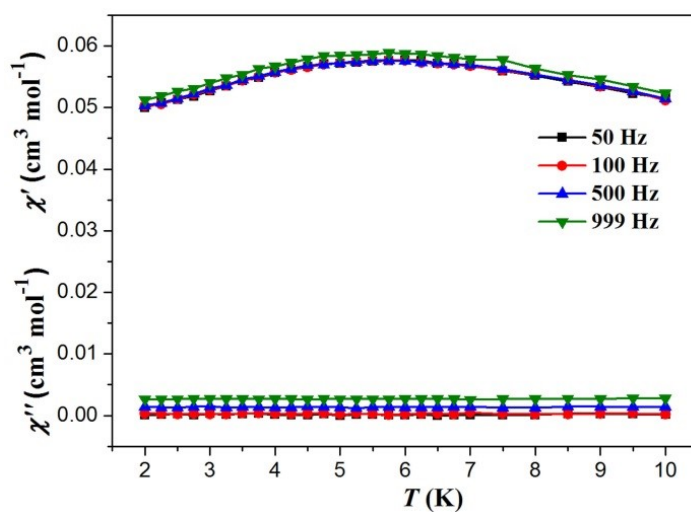


Fig. S19 Temperature dependence of the in-phase (χ') and out-of-phase (χ'') ac susceptibilities for **1** between 2 and 10 K at the indicated frequencies and in zero dc field.

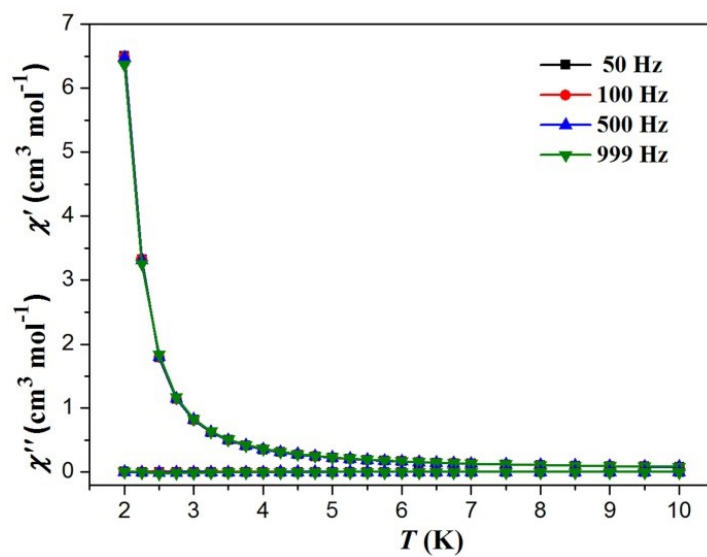


Fig. S20 Temperature dependence of the in-phase (χ') and out-of-phase (χ'') ac susceptibility for **2** at the indicated frequencies and in zero dc field.